

1 **A New Algorithm for Incidental Pancreatic Cyst Detection**

2

3 M. Álvaro Berbís<sup>1</sup>, Juan Moreno-Vedia<sup>2</sup>, Félix Paulano-Godino<sup>1</sup>, Ainhoa Viteri<sup>1</sup>, Meritxell  
4 Riera-Marín<sup>2</sup>, Daniel Cañadas-Gómez<sup>2</sup>, Romina Trotta<sup>1</sup>, Beatriz Forastero<sup>1</sup>, Luis Luna<sup>1</sup>,  
5 Javier García López<sup>2</sup>, Antonio Luna<sup>3</sup>, Júlia Rodríguez-Comas<sup>2</sup>

6

7 <sup>1</sup> Department of Radiology, HT Médica, San Juan de Dios Hospital, 14012 Córdoba, Spain.

8 <sup>2</sup> Scientific and Technical department, Sycal Technologies S.L., 08018 Barcelona, Spain.

9 <sup>3</sup> Department of Radiology, HT Médica, Clínica las Nieves, 23007, Jaén, Spain

10

11

12 **Corresponding author:**

13 M. Álvaro Berbís, PhD

14 Radiology Department, HT Médica, Hospital San Juan de Dios de Córdoba

15 Avda. Brillante 106, 14012 Córdoba, Spain

16 [a.berbis@htime.org](mailto:a.berbis@htime.org)

17

18

19 **ABSTRACT**

20 **Objectives:** To develop an accurate, state-of-the-art algorithm for the incidental detection of  
21 pancreatic cystic lesions (PCLs) on computerized tomography (CT) and magnetic resonance  
22 imaging (MRI) scans.

23 **Methods:** A SwinT-Unet-based architecture was developed for the incidental detection of  
24 PCLs. The algorithm was trained and validated on a robust dataset of retrospective CT and  
25 MRI studies collected from HT Médica centers located in eight different cities using scanners  
26 fabricated by four different manufacturers.

27 **Results:** Our algorithm was able to detect 91.6% of the confirmed PCLs in the initial dataset  
28 with 91.6% sensitivity and 92.3% specificity, while 91.7% of the healthy controls were also  
29 correctly identified. Furthermore, our tool was remarkably capable of classifying these PCLs  
30 as mucinous or non-mucinous, determining their location within the pancreas with an  
31 accuracy of 88.5%, and identifying the presence of calcifications or scars within the PCLs  
32 with an accuracy of 96%.

33 **Conclusions:** By integrating radiological data and state-of-the-art artificial intelligence  
34 techniques, we have developed an efficient tool for the incidental identification and initial  
35 characterization of PCLs, which present a substantial prevalence within the global  
36 population. Our algorithm facilitates early diagnosis of pancreatic abnormalities, which could  
37 have a profound impact on patient management and prognosis, particularly in the case of  
38 PCLs with malignant potential.

39

40 **Keywords:** Pancreatic Cysts, Computerized Tomography, Magnetic Resonance Imaging,  
41 Incidental Findings, Artificial Intelligence, SwinT-Unet.

42

## 43 INTRODUCTION

44 Pancreatic cancer (PC) currently ranks as the twelfth most common type of cancer globally  
45 [1], and it is further expected to become the second leading cause of cancer-related mortality  
46 by 2030 [2]. Moreover, PC is one of the most lethal types of cancer, with a 5-year survival  
47 rate inferior to 10% [3]. The delayed onset of PC symptoms, often appearing when metastasis  
48 has already occurred, results in up to 85% of patients no longer being eligible for surgical  
49 resection, which has a profound negative impact on their prognosis [4,5].

50 Many research efforts are currently focused on the identification of biomarkers for early PC  
51 detection, aiming to improve patient outcomes. However, only one of these biomarkers, the  
52 serum carbohydrate antigen 19-9, has been approved by the US Food and Drug  
53 Administration (FDA), and only as a therapy response and disease relapse monitoring  
54 marker, as its predictive value is too low for population screening purposes [6]. Nonetheless,  
55 there is an opportunity for early PC diagnosis in patients presenting pancreatic cystic lesions  
56 (PCLs), as some of them are well-known precursors for this malignancy. The widespread  
57 adoption of advanced imaging techniques, particularly computed tomography (CT) and  
58 magnetic resonance imaging (MRI), has led to an increased identification of conditions  
59 unrelated to the initially suspected diagnosis. These incidental findings can indeed be  
60 fortunate discoveries when they entail the early detection of a potentially treatable  
61 malignancy. Unsuspected PCLs have a prevalence of 2.6% in CT scans [7] and of 13.5–  
62 19.6% in MRI studies [8,9], and both show a strong correlation with advanced age.  
63 Unexpectedly, a recent study found a much higher prevalence (49.1%) of incidental PCLs in  
64 healthy individuals, which also increased with body mass index and age [10].

65 PCLs can have a non-neoplastic (pseudocysts) or a neoplastic nature. Among the latter,  
66 serous cystadenomas (SCA) are typically regarded as benign [11], while mucinous cysts are  
67 often associated with malignant potential. Intraductal papillary mucinous neoplasms (IPMN)  
68 and mucinous cystic neoplasms (MCN) are two well-known PC precursors. IPMNs can arise  
69 from the side branches, the main pancreatic duct, or a combination of both, with a notably  
70 higher prevalence of PC found in main duct IPMNs [12]. Thus, this distinction has a direct  
71 impact on patient management and prognosis. PC cases arising from PCLs have been  
72 proposed to follow a systematic model in which malignancy progression occurs over several  
73 years, thus offering an opportunity for early diagnosis [13,14]. However, differentiation  
74 between the different types of PCLs is challenging, and although the presence of some  
75 specific features can be indicative of malignancy [15,16], these signs are sometimes not  
76 enough to confidently distinguish between benign and malignant PC precursors.  
77 Nevertheless, early detection of PCLs is essential to improve patient outcomes and reduce  
78 the economic strain on healthcare systems, as it would allow more informed, enhanced  
79 decision-making regarding lesion management and monitoring, thus potentially preventing  
80 progression to PC.

81 Artificial intelligence (AI) tools are poised to play a crucial role in the early detection of  
82 PCLs in CT and MR images. These algorithms have the potential to accurately identify and  
83 define lesion boundaries and to extract essential qualitative and quantitative information from  
84 their features, thus improving diagnostic precision. The implementation of these tools would  
85 also help to streamline the workflow in radiology departments, providing valuable assistance  
86 to radiologists in the diagnostic process and reducing their workload. The capability of  
87 convolutional neural networks (CNNs) to learn the spatial hierarchies of features from input

88 data in an automatic and adaptive manner makes them exceptionally useful for extracting  
89 information from medical images. This capability allows CNNs to learn complex patterns at  
90 different levels of abstraction, recognize patterns independently of their spatial location, and  
91 even identify new patterns not obvious to the human eye. Moreover, depending on the  
92 specific dataset they are trained on, CNNs can work with multiple types of imaging studies  
93 (ultrasound, CT, MRI, etc.) and perform a wide variety of tasks (detection, segmentation,  
94 classification, etc.). Applied to medical images, the AI model presented in this manuscript,  
95 based on the SwinT-Unet architecture, offers exceptional segmentation accuracy and  
96 remarkable generalization ability, allowing the discrimination of structures at the pixel level.  
97 The results showed an outstanding performance of our algorithm, achieving 91.6%  
98 sensitivity and 92.3% specificity in the incidental detection of PCLs, while also  
99 demonstrating a remarkable capacity to further characterize the lesion by classifying it as  
100 mucinous or non-mucinous, accurately determining its location within the pancreas, and  
101 identifying the presence of calcifications or scars within the PCLs. Our findings confirm a  
102 significant prevalence of PCLs within our study population, highlighting the crucial support  
103 a tool like ours might provide through the early diagnosis of pancreatic abnormalities and the  
104 significant impact this would have on patient management and prognosis, particularly in the  
105 case of PLCs with malignant potential.

106

## 107 **MATERIALS AND METHODS**

108 *Patients*

109 The total cohort included 43.3% women (**table 1**). This initial cohort was divided into two  
110 subgroups: the control group included 56.3% of the patients (37.9% women, **table 2**), while  
111 the second group, comprising patients who had been diagnosed with a PCL, included 43.7%  
112 of the study population (**table 3**). Both groups showed a similar age distribution, and women  
113 and men were equally represented in the PCL group, which was further characterized to  
114 analyze the performance of our algorithm.

115

### 116 *Imaging*

117 Image studies were acquired at different HT Médica medical centers located in the Spanish  
118 cities of Jaén, Córdoba, El Ejido, Huelva, Cádiz, Jerez de la Frontera, Algeciras, and Sevilla,  
119 from January 2018 to December 2021, using scanners developed by the following  
120 manufacturers (**tables 1–3**): Canon Medical Systems (Otawara, Japan), GE Healthcare  
121 (Chicago, IL, United States), Philips (Amsterdam, The Netherlands), and Siemens  
122 Healthineers (Erlangen, Germany). Demographic data of the patients, including age and  
123 gender, were collected from HT Médica’s radiological information system.

124

### 125 *Segmentation and feature extraction*

126 A team of radiologists, each of them with more than five years of experience, manually  
127 delineated the pancreas and PCLs in all the images, slice by slice, using the 3D modeling tool  
128 available in the Philips IntelliSpace Portal (v12.1). The segmentations were subsequently  
129 exported in RTSTRUCT format. To ensure agreement between raters, collaborative

130 segmentation, and consensus resolution were employed, minimizing discrepancies in the  
131 assessment process.

132

### 133 *Algorithm development*

134 The proposed model (**fig1**) is based on the SwinT-Unet [17] architecture, a further  
135 development from the U-Net [18] that aims to predict objects on an image with pixel-wise  
136 accuracy. Our model includes an encoder block, to reduce input resolution, and a U-Net  
137 decoder with dual-scale information modules. The encoder is an attention-based model with  
138 blocks that capture information at multiple scales, similar to that proposed by Atek et al. [17].  
139 The input image is processed through multiple Swin transformer blocks performing attention  
140 operations and feature transformation. These blocks are responsible for feature extraction at  
141 various scales, allowing the model to capture both the fine details and high-level abstract  
142 features. After information passes through the encoder, the architecture adopts a U-Net-like  
143 structure [18] to perform segmentation. The decoder takes the features extracted by the  
144 encoder and uses them to generate a segmentation mask of the same resolution as the original  
145 input. Additionally, the decoder incorporates dual-scale information modules to merge  
146 features from different resolution levels that allow the model to integrate detailed and  
147 contextual information at different scales, thus improving segmentation accuracy, especially  
148 in areas with fine details or small features. This ability to process features and key points at  
149 different levels is crucial for the network to learn the features that best characterize big  
150 organs, such as the liver, as well as small lesions with different shapes and textures, such as  
151 PCLs. The network was specifically trained to learn the position and shape of the liver,  
152 kidneys, and pancreas, as well as a wide range of benign, pre-malignant, and malignant



153 lesions present in the training set corresponding to the aforementioned organs. The model  
154 proposed here further includes two more steps: (1) a pre-processing step, prior to the  
155 inference of the neural network, that normalizes the input image by applying a Soft-Tissue  
156 Normalization [19], and (2) a post-processing step after the inference the filters out potential  
157 detections of the network that have no anatomical meaning, such as lesions belonging to an  
158 organ which they are not in direct contact with or predictions present in parts of the study  
159 where the abdomen is not visible yet.

160

### 161 *Statistical analysis*

162 The Kolmogorov–Smirnov test was used to assess normality. Categorical variables are  
163 presented as total numbers and percentages, and continuous variables are presented as  
164 medians and interquartile ranges (IQRs) for non-normally distributed data. The chi-square  
165 ( $\chi^2$ ) test was used to analyze group differences for categorical variables, while the Mann–  
166 Whitney U test was used for continuous variables. Results were considered statistically  
167 significant if  $p < 0.05$ . Statistical analyses were conducted using the SPSS Statistics, version  
168 29.0.0.0 (IBM, Armonk, NY, United States).

169

## 170 **RESULTS**

### 171 *Patient's characteristics*

172 The median age of the patients included in the present study was 66 years old. The 61–80  
173 age range was the most represented, consistent with the expected increase in CT and MRI  
174 scans performed as the population ages. Women accounted for 43.3% of the initially

175 evaluated patients (**table 1**). The recruited cohort was divided into two groups: one group  
176 with confirmed PCLs, including 43.7% of the patients, and a control group of healthy  
177 individuals. Both groups showed a similar age distribution, and women and men were equally  
178 represented in the PCL group (**tables 2 and 3**).

179 Among these PCL lesions, 61.1% of them were identified as non-mucinous (serous cystic  
180 neoplasms (SCN), pseudocysts) and 38.9% were classified as mucinous (MCNs, IPMNs).  
181 Within the non-mucinous group, 93.8% of them were SCNs or pseudocysts; additionally,  
182 3.8% of non-subclassified benign lesions and 2.5% of undetermined non-mucinous lesions  
183 were detected (**table 4**). The prevalence of both mucinous and non-mucinous lesions  
184 increased with age, with mucinous cases associated with a higher median age ( $p<0.001$ ).  
185 Notably, a higher percentage of patients with mucinous lesions fell within the 61–80 age  
186 range, consistent with the expectation of a higher lesion incidence in older patients [10].

187

### 188 *Incidental finding of PCLs*

189 Out of the initial dataset, 43.7% of the cases were confirmed as true positives for a PCL,  
190 based on radiological evidence. This prevalence is in alignment with the existing literature,  
191 which reports the presence of PCLs in up to 49.1% of the adult population [10]. Our  
192 algorithm successfully detected 91.6% of the lesions, while 8.4% were missed (false  
193 negatives). Furthermore, among the control population, the algorithm accurately identified a  
194 healthy pancreas in 91.7% of the cases but presented 7.7% of false positives.

195 Overall, our SwinT-Unet-based model showed 91.6% sensitivity and 92.3% specificity in the  
196 detection of PCLs. These results confirm the high precision and reliability of our AI-based

197 approach in distinguishing between cystic lesions and non-cystic structures within the  
198 pancreas, underscoring the potential of AI technology to enhance the accuracy and efficiency  
199 of pancreatic lesion detection, thereby facilitating early diagnosis and treatment planning for  
200 patients with pancreatic abnormalities.

201

### 202 *Characterization of PCLs: mucinous vs. non-mucinous classification and location*

203 While the majority of pancreatic cysts carry a low risk of malignancy, some are recognized  
204 as premalignant lesions capable of progressing into mucin-producing adenocarcinoma.  
205 Consequently, the identification of these cysts often triggers heightened anxiety in the patient  
206 and prompts additional medical investigations to assess the potential for malignancy [20,21].

207 While the primary objective in this study was the incidental detection of PCLs, the  
208 classification of these cysts as mucinous (IPMNs, MCNs) or non-mucinous (SCNs,  
209 pseudocysts) [22] was also addressed, achieving an accuracy of 73.3% in the classification  
210 of PLCs as mucinous (**fig2**).

211 Furthermore, we analyzed the spatial distribution of the PCLs within the pancreas, with the  
212 algorithm demonstrating a high accuracy (88.5%) in categorizing the cysts as head, body, or  
213 tail, according to their location. Specifically, the algorithm was capable of correctly  
214 determining the location of the lesion at the head or the uncinate process of the pancreas with  
215 an accuracy of 86%, at the body with an accuracy of 92.6%, and at the tail with an accuracy  
216 of 75.7%.

217 Additionally, we conducted a thorough examination for the presence of calcifications or scars  
218 within the cystic lesions, achieving an accuracy of 96% in their identification. This was

219 crucial to assess the presence of potential signs of malignancy or chronic inflammation within  
220 the PCL. To achieve this, several image feature extraction algorithms were applied to study  
221 the high increments of Hounsfield Units (HU) on small sliding windows passed through  
222 patches of the image where the lesion was detected. A map of the increased direction of the  
223 HU within the sliding window is thus generated and, by calculating its maximum, the  
224 candidates to potential scars (understood as groups of pixels with a high HU, since they have  
225 a great bone component that is aligned towards a defined direction within the PCL) are  
226 extracted.

227 This comprehensive characterization of the PCL provides valuable insights into the diverse  
228 nature of the lesion, supporting clinicians in diagnostic decision-making and risk  
229 stratification for further management strategies.

230

## 231 **DISCUSSION**

232 Considerable efforts have been employed to try to distinguish between the different types of  
233 PCLs, as this step is essential to correctly stratify the malignant potential of the lesion so the  
234 best patient management can be provided. Duh et al. developed an AG-Net model capable of  
235 identifying PCLs on CT scans with 93.1% sensitivity and 81.8% specificity, further  
236 classifying them into two groups (IPMN and MCN vs pseudocysts and SCAs) [23]. Vilas-  
237 Boas et al. designed a CNN for the automatic detection of mucinous PCLs. The algorithm,  
238 trained on images retrieved from EUS examination videos, achieved 98.5% accuracy, 98.3%  
239 sensitivity, and 98.9% specificity in the classification of PCLs as mucinous or non-mucinous  
240 [24]. Yang et al. developed a random forest (RF) model capable of differentiating between

241 serous and mucinous pancreatic cystadenomas based on the analysis of radiomics texture  
242 features extracted from CT scans. Their algorithm achieved 0.83 accuracy, 0.85 sensitivity,  
243 and 0.83 specificity for a slice thickness of 5 mm [25]. Shen et al. compared the performance  
244 of a support vector machine (SVM) model, an RF algorithm, and an artificial neural network  
245 (ANN) in differentiating among SCAs, MCNs, and IPMNs using eight clinical factors and  
246 nine radiomics features extracted from CT scans [26]. The RF classifier offered the best  
247 results, achieving an accuracy of 79.59% and F1 scores of 0.7500 for the differentiation of  
248 IPMNs, 0.8182 for MCNs, and 0.8077 for SCAs. Gao et al. designed a CNN to identify  
249 pancreatic anomalies, including PCLs, on MRI images [27]. The authors employed 504  
250 original pre-treatment MRI studies to train their model. As most of the patches within the  
251 images corresponded to carcinoma, they augmented the number of images for the other  
252 conditions with the help of a generative adversarial network (GAN), creating synthetic  
253 images based on real ones up to a total of 35735 patches for the training dataset. The CNN  
254 trained on this augmented dataset offered its best results when a synthetic to real images ratio  
255 of 40:1 was used, achieving an AUC of 0.9147 for the identification of carcinomas, 0.8486  
256 for benign ductal diseases, 0.9126 for benign cystic diseases, 0.7189 for inflammatory  
257 diseases, 0.9301 for pancreatic neuroendocrine tumors, and 0.8880 for solid pseudopapillary  
258 tumors.

259 The number of studies exploring the incidental finding of PCLs via AI approaches is much  
260 reduced. Kooragayala et al. employed a publicly available natural language processing (NLP)  
261 software to identify incidental findings on CT scan reports [28]. The authors created a list of  
262 specific terms (including IPMN, pancreatic cyst, and pancreatic ductal dilation) to identify  
263 pancreatic findings that were used as parameters to train the algorithm on a subset of 28

264 patients who had undergone pancreatic resection for known pancreatic lesions. This  
265 algorithm achieved an accuracy of 0.987 on a validation set of 400 CT scan reports. Their  
266 optimized model was subsequently applied to 18769 CT studies from patients admitted at  
267 their institution for trauma and findings of interest were identified in 232 of them, including  
268 potential IMPNs (48 patients), pancreatic cysts (36 patients), concerning masses (30  
269 patients), traumatic findings (44 patients), pancreatitis (41 patients), and ductal abnormalities  
270 (19 patients).

271 By utilizing CT and MRI scans originally intended for the identification or evaluation of  
272 conditions not related to pancreatic abnormalities, the algorithm we present in this study  
273 offers a novel approach to the detection of PCLs. Our tool confirmed the incidental presence  
274 of PCLs in 43.7% of the study population, in accordance with previously reported data [10].  
275 Out of all confirmed cases, the SwinT-UNET-based algorithm correctly identified 91.6% of  
276 them with a remarkable 91.6% sensitivity and 92.3% specificity, improving the results  
277 reported by Duh et al., which were obtained with an algorithm specifically designed for the  
278 classification of PCLs, not for their incidental detection. Furthermore, our algorithm is  
279 capable of providing a comprehensive characterization of the PCL through its classification  
280 as mucinous or non-mucinous with 73.3% accuracy. Although this result did not improve  
281 those previously reported [24–27], the tool presented here can further characterize the PCL  
282 by categorizing the lesion according to its location in the head, body, or tail of the pancreas  
283 with 88.5% accuracy, as well as identifying the presence of calcifications or scars within the  
284 PCL with 96% accuracy. Taken together, all this information provides a comprehensive  
285 characterization of the lesion that, without any doubt, will be very valuable to clinicians for  
286 the planning of tailored patient management strategies.

287 The results presented in this study were achieved using a robust dataset consisting of CT and  
288 MRI studies obtained from eight different medical centers using scanners fabricated by four  
289 different manufacturers. However, they are limited by the somewhat reduced number of  
290 imaging studies included.

291

## 292 **CONCLUSIONS**

293 Our study presents comprehensive findings regarding the incidental detection and  
294 characterization of PCLs through the integration of radiological data and advanced AI  
295 techniques. The results reveal a substantial prevalence of PCLs within the studied population,  
296 highlighting the importance of thorough radiological evaluations in clinical practice.

297 Our AI model, based on the SwinT-Unet architecture, showed a remarkable performance in  
298 detecting PCLs with a sensitivity of 91.6% and a specificity of 92.3%. Furthermore, our study  
299 contributes to the in-depth characterization of PCLs by distinguishing between mucinous and  
300 non-mucinous types, aiding in risk stratification and clinical decision-making, and the  
301 identification of calcifications or scars within the cystic lesions, an aspect crucial for the  
302 assessment of potential signs of malignancy or chronic inflammation within the PCL. These  
303 outcomes not only emphasize the clinical utility of our approach but also highlight the  
304 potential of AI-driven approaches in enhancing the accuracy and efficiency of pancreatic  
305 lesion detection, which will undoubtedly have a profound impact on patient management and  
306 prognosis, particularly in the case of PCLs with malignant potential.

307

308

309 **DECLARATIONS**

310 **Funding**

311 This project was co-financed by the European Union (NextGenerationEU) through the Public  
312 Business Entity Red.es, affiliated to the Secretaría de Estado de Digitalización e Inteligencia  
313 Artificial, Ministerio de Asuntos Económicos y Transformación Digital (Secretary of State  
314 for Digitalization and Artificial Intelligence, Ministry of Economic Affairs and Digital  
315 Transformation) within the framework of the 2021 Call for Aid for research and development  
316 projects in artificial intelligence and other digital technologies and their integration into value  
317 chains (C005/21-ED call, project reference 2021/C005/00153960).

318

319 **Competing interests**

320 M. Álvaro Berbís is the CEO of Cells IA Technologies. Antonio Luna received institutional  
321 royalties and institutional payments for lectures, presentations, speakers bureaus, manuscript  
322 writing, or educational events from Canon, Bracco, Siemens Healthineers, and Philips  
323 Healthcare and is a board member of Cells IA Technologies. Júlia Rodríguez-Comas is the  
324 CTO of Sycal Technologies. The remaining authors have no competing interests to declare  
325 that are relevant to the content of this article.

326

327 **Ethics approval**



328 This research was performed in accordance with the ethical standards in the 1964 Declaration  
329 of Helsinki. The protocol followed in this study was approved by the Institutional Review  
330 Board of HT Médica.

331

### 332 **Consent**

333 Written informed consent was obtained from the patients at the time of the performance of  
334 the imaging study.

335

### 336 **Data, Materials, and/or Code availability**

337 The data used in this study are not openly available due to commercial and proprietary  
338 constraints. Access to the data may be granted by the corresponding author upon reasonable  
339 request and subject to confidentiality agreements.

340

### 341 **Authors' contributions**

342 Study conception and design were performed by M. Álvaro Berbís and Júlia Rodríguez-  
343 Comas. Material preparation, data collection, and analysis were performed by M. Álvaro  
344 Berbís, Juan Moreno-Vedia, Félix Paulano-Godino, Ainhoa Viteri, Meritxell Riera-Marín,  
345 Daniel Cañadas-Gómez, Romina Trotta, Beatriz Forastero, Luis Luna, and Javier García  
346 López. Supervision was performed by M. Álvaro Berbís and Júlia Rodríguez-Comas. The  
347 first draft of the manuscript was written by M. Álvaro Berbís, Javier García López and Júlia  
348 Rodríguez-Comas. Manuscript review and editing was performed by Antonio Luna. All

349 authors commented on previous versions of the manuscript. All authors read and approved  
350 the final manuscript.

351

## 352 REFERENCES

- 353 1. Sung H, Ferlay J, Siegel RL, Laversanne M, Soerjomataram I, Jemal A, et al. Global Cancer  
354 Statistics 2020: GLOBOCAN Estimates of Incidence and Mortality Worldwide for 36 Cancers in 185  
355 Countries. *CA Cancer J Clin.* 2021;71:209–49.
- 356 2. Rahib L, Smith BD, Aizenberg R, Rosenzweig AB, Fleshman JM, Matrisian LM. Projecting Cancer  
357 Incidence and Deaths to 2030: The Unexpected Burden of Thyroid, Liver, and Pancreas Cancers in  
358 the United States. *Cancer Res.* 2014;74:2913–21.
- 359 3. Siegel RL, Miller KD, Jemal A. Cancer statistics, 2020. *CA Cancer J Clin.* 2020;70:7–30.
- 360 4. Bengtsson A, Andersson R, Ansari D. The actual 5-year survivors of pancreatic ductal  
361 adenocarcinoma based on real-world data. *Sci Rep.* 2020;10:16425.
- 362 5. Vincent A, Herman J, Schulick R, Hruban RH, Goggins M. Pancreatic cancer. *The Lancet.*  
363 2011;378:607–20.
- 364 6. Kim J, Lee KT, Lee JK, Paik SW, Rhee JC, Choi KW. Clinical usefulness of carbohydrate antigen 19-9  
365 as a screening test for pancreatic cancer in an asymptomatic population. *J Gastroenterol Hepatol.*  
366 2004;19:182–6.
- 367 7. Laffan TA, Horton KM, Klein AP, Berlanstein B, Siegelman SS, Kawamoto S, et al. Prevalence of  
368 Unsuspected Pancreatic Cysts on MDCT. *American Journal of Roentgenology.* 2008;191:802–7.
- 369 8. Zhang X-M, Mitchell DG, Dohke M, Holland GA, Parker L. Pancreatic Cysts: Depiction on Single-  
370 Shot Fast Spin-Echo MR Images. *Radiology.* 2002;223:547–53.
- 371 9. Lee KS, Sekhar A, Rofsky NM, Pedrosa I. Prevalence of Incidental Pancreatic Cysts in the Adult  
372 Population on MR Imaging. *American Journal of Gastroenterology.* 2010;105:2079–84.
- 373 10. Kromrey M-L, Bülow R, Hübner J, Paperlein C, Lerch MM, Ittermann T, et al. Prospective study  
374 on the incidence, prevalence and 5-year pancreatic-related mortality of pancreatic cysts in a  
375 population-based study. *Gut.* 2018;67:138–45.
- 376 11. Jais B, Rebours V, Malleo G, Salvia R, Fontana M, Maggino L, et al. Serous cystic neoplasm of  
377 the pancreas: a multinational study of 2622 patients under the auspices of the International  
378 Association of Pancreatology and European Pancreatic Club (European Study Group on Cystic  
379 Tumors of the Pancreas). *Gut.* 2016;65:305–12.
- 380 12. Tanaka M, Chari S, Adsay V, Carlos Castillo F-D, Falconi M, Shimizu M, et al. International  
381 Consensus Guidelines for Management of Intraductal Papillary Mucinous Neoplasms and  
382 Mucinous Cystic Neoplasms of the Pancreas. *Pancreatology.* 2006;6:17–32.
- 383 13. Maitra A, Adsay NV, Argani P, Iacobuzio-Donahue C, De Marzo A, Cameron JL, et al.  
384 Multicomponent Analysis of the Pancreatic Adenocarcinoma Progression Model Using a Pancreatic  
385 Intraepithelial Neoplasia Tissue Microarray. *Modern Pathology.* 2003;16:902–12.
- 386 14. Yachida S, Jones S, Bozic I, Antal T, Leary R, Fu B, et al. Distant metastasis occurs late during the  
387 genetic evolution of pancreatic cancer. *Nature.* 2010;467:1114–7.

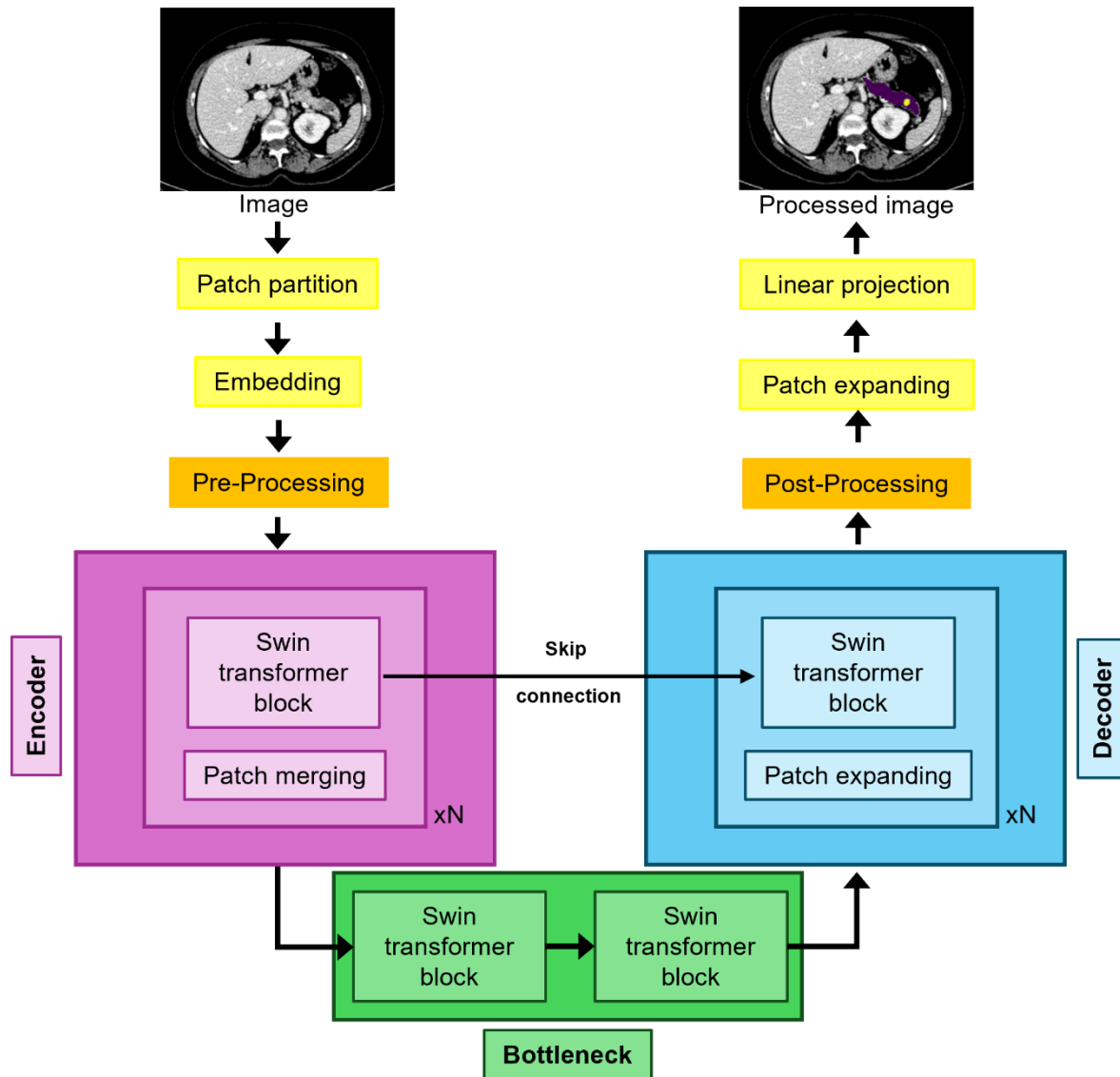
- 388 15. European evidence-based guidelines on pancreatic cystic neoplasms. *Gut*. 2018;67:789–804.
- 389 16. Tanaka M, Fernández-del Castillo C, Kamisawa T, Jang JY, Levy P, Ohtsuka T, et al. Revisions of  
390 international consensus Fukuoka guidelines for the management of IPMN of the pancreas.  
391 *Pancreatology*. 2017;17:738–53.
- 392 17. Atek S, Mehidi I, Jabri D, Belkhiat DEC. SwinT-Unet: Hybrid architecture for Medical Image  
393 Segmentation Based on Swin transformer block and Dual-Scale Information. 2022 7th International  
394 Conference on Image and Signal Processing and their Applications (ISPA). IEEE; 2022. p. 1–6.
- 395 18. Ronneberger O, Fischer P, Brox T. U-Net: Convolutional Networks for Biomedical Image  
396 Segmentation. In: Navab N, Hornegger J, Wells WFA, editors. *Medical Image Computing and  
397 Computer-Assisted Intervention – MICCAI 2015 MICCAI 2015 Lecture Notes in Computer Science()*.  
398 2015. p. 234–41.
- 399 19. Huo Y, Tang Y, Chen Y, Gao D, Han S, Bao S, et al. Stochastic tissue window normalization of  
400 deep learning on computed tomography. *Journal of Medical Imaging*. 2019;6:1.
- 401 20. Polk SL, Choi JW, McGettigan MJ, Rose T, Ahmed A, Kim J, et al. Multiphase computed  
402 tomography radiomics of pancreatic intraductal papillary mucinous neoplasms to predict  
403 malignancy. *World J Gastroenterol*. 2020;26:3458–71.
- 404 21. Anand N, Sampath K, Wu BU. Cyst features and risk of malignancy in intraductal papillary  
405 mucinous neoplasms of the pancreas: A meta-analysis. *Clinical Gastroenterology and Hepatology*.  
406 2013;11:913–21.
- 407 22. Udare A, Agarwal M, Alabousi M, McInnes M, Rubino JG, Marcaccio M, et al. Differentiation of  
408 Benign and Malignant Pancreatic Cystic Lesions Compared to CT and Endoscopic Ultrasound:  
409 Systematic Review and Meta-analysis. *J Magn Reson*. 2021;
- 410 23. Duh MM, Torra-Ferrer N, Riera-Marín M, Cumelles D, Rodríguez-Comas J, García López J, et al.  
411 Deep Learning to Detect Pancreatic Cystic Lesions on Abdominal Computed Tomography Scans:  
412 Development and Validation Study. *JMIR AI*. 2023;2:e40702.
- 413 24. Vilas-Boas F, Ribeiro T, Afonso J, Cardoso H, Lopes S, Moutinho-Ribeiro P, et al. Deep Learning  
414 for Automatic Differentiation of Mucinous versus Non-Mucinous Pancreatic Cystic Lesions: A Pilot  
415 Study. *Diagnostics*. 2022;12:2041.
- 416 25. Yang J, Guo X, Ou X, Zhang W, Ma X. Discrimination of Pancreatic Serous Cystadenomas From  
417 Mucinous Cystadenomas With CT Textural Features: Based on Machine Learning. *Front Oncol*.  
418 2019;9.
- 419 26. Shen X, Yang F, Yang P, Yang M, Xu L, Zhuo J, et al. A Contrast-Enhanced Computed Tomography  
420 Based Radiomics Approach for Preoperative Differentiation of Pancreatic Cystic Neoplasm  
421 Subtypes: A Feasibility Study. *Front Oncol*. 2020;10.
- 422 27. Gao X, Wang X. Performance of deep learning for differentiating pancreatic diseases on  
423 contrast-enhanced magnetic resonance imaging: A preliminary study. *Diagn Interv Imaging*.  
424 2020;101:91–100.

425 28. Kooragayala K, Crudeli C, Kalola A, Bhat V, Lou J, Sensenig R, et al. Utilization of Natural  
426 Language Processing Software to Identify Worrisome Pancreatic Lesions. *Ann Surg Oncol*.  
427 2022;29:8513–9.

428

429

430 **FIGURES**

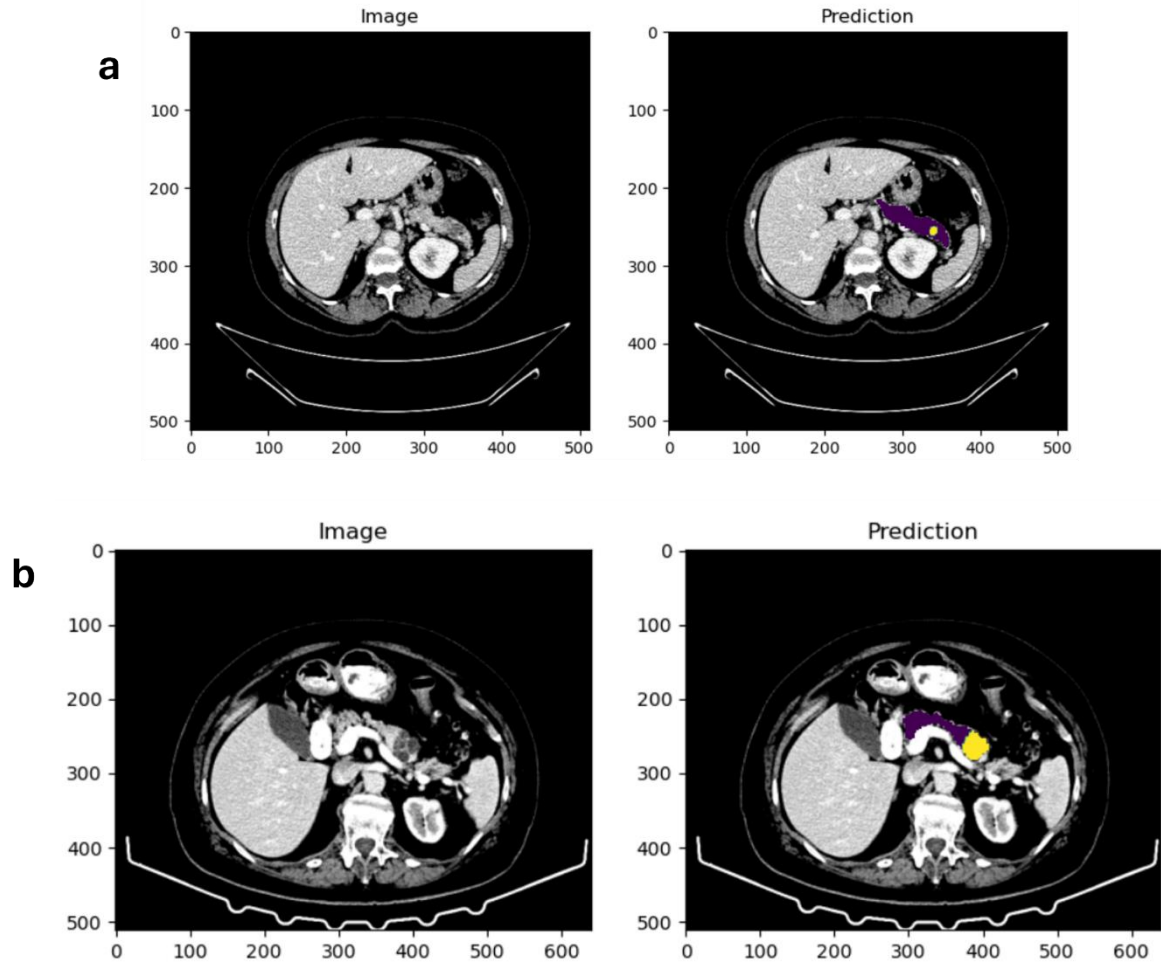


431

432 **Fig1. Schematic representation of the Swin-Unet architecture.** The algorithm integrates  
433 a Swin transformer-based encoder and a symmetrical Swin transformer-based decoder,  
434 connected by two successive Swin transformer blocks (bottleneck).

435

436



437

438 **Fig2. Original images and predictions made by our algorithm. (A) Mucinous PCL. (B)**

439 **Non-mucinous PCL. Healthy pancreas is shown in purple, while the lesions appear in yellow.**

440

441

442 **TABLES**

443 **Table 1. Demographic and manufacturer distribution of the total cases included in the study.**

	<b>Total Cases</b>	<b><i>p</i></b>
<b>Age (years)</b>	66 (55-74)	
0-18	0	<b>&lt;0.001</b>
19-40	3.7%	
41-60	32%	
61-80	60%	
81-100	4.3%	
<b>Women</b>	43.3%	<b>0.021</b>
<b>Manufacturer</b>		<b>&lt;0.001</b>
Siemens	47%	
Philips	26.3%	
GE Medical systems	15.7%	
Canon Medical Systems	11%	

444

445



446 **Table 2. Demographic and manufacturer distribution of the control cases included in the study.**

	<b>Control Cases</b>	<b><i>p</i></b>
<b>Age (years)</b>	65 (56-72)	
0-18	0	<b>&lt;0,001</b>
19-40	4.1 %	
41-60	32%	
61-80	61.2%	
81-100	1.8%	
<b>Women</b>	37.9%	<b>0.002</b>
<b>Manufacturer</b>		<b>&lt;0,001</b>
Siemens	40.8%	
Philips	27.8%	
GE Medical systems	16%	
Canon Medical Systems	15.4%	

447

448

449

450

451

452

453

454 **Table 3. Demographic and manufacturer distribution of the PCL cases included in the study.**

	<b>PCL Cases</b>	<b><i>p</i></b>
<b>Age (years)</b>	68 (54-76)	
0-18	0	<b>&lt;0.001</b>
19-40	3.1%	
41-60	32.1%	
61-80	57.3%	
81-100	7.6%	
<b>Women</b>	50.4%	0.930
<b>Manufacturer</b>		<b>&lt;0.001</b>
Siemens	55%	
Philips	24.4%	
GE Medical systems	15.3%	
Canon Medical Systems	5.3%	

455 PCL: Pancreatic Cystic Lesion

456

457 **Table 4. Clinical and demographic characteristics of mucinous and non-mucinous PCLs.**

	<b>Mucinous PCL</b>	<b>Non-mucinous PCL</b>	<b><i>p</i></b>
SCN	-	70%	
Pseudocyst	-	23.8%	
Benign non-subclassifiable	-	3.8%	
Undetermined	-	2.5%	
IPMN	90.2%	-	
MCN	9.8%	-	
<b>Age (years)</b>	<b>72 (64-79)</b>	<b>63 (51-74)</b>	<b>&lt;0.001</b>
0-18	0	0	
19-40	0	5%	
41-60	19.6%	40%	
61-80	68.6%	50%	
81-100	11.8%	5%	
<b>Women</b>	<b>54.9%</b>	<b>47.5%</b>	<b>0.409</b>

458 PCL: Pancreatic Cystic Lesion; SCN: Serous Cystic Neoplasms; IPMN: Intraductal Papillary Mucinous  
 459 Neoplasms; MCN: Mucinous Cystic Neoplasms.

460

461

462